Journal of Biomedical Optics

BiomedicalOptics.SPIEDigitalLibrary.org

Optimization of image reconstruction for magnetic resonance imaging–guided near-infrared diffuse optical spectroscopy in breast

Yan Zhao
Michael A. Mastanduno
Shudong Jiang
Fadi EI-Ghussein
Jiang Gui
Brian W. Pogue
Keith D. Paulsen

SPIE.

Optimization of image reconstruction for magnetic resonance imaging–guided near-infrared diffuse optical spectroscopy in breast

Yan Zhao,[a,*] Michael A. Mastanduno,[a] Shudong Jiang,[a] Fadi El-Ghussein,[a] Jiang Gui,[b] Brian W. Pogue,[a] and Keith D. Paulsen[a,b,c]
[a]Dartmouth College, Thayer School of Engineering, Hanover, New Hampshire 03755, United States
[b]Dartmouth College, Geisel School of Medicine, Department of Community and Family Medicine, Hanover, New Hampshire 03755, United States
[c]Dartmouth College, Geisel School of Medicine, Department of Diagnostic Radiology, Hanover, NH03755, United States

Abstract. An optimized approach to nonlinear iterative reconstruction of magnetic resonance imaging (MRI)–guided near-infrared spectral tomography (NIRST) images was developed using an L-curve-based algorithm for the choice of regularization parameter. This approach was applied to clinical exam data to maximize the reconstructed values differentiating malignant and benign lesions. MRI/NIRST data from 25 patients with abnormal breast readings (BI-RADS category 4-5) were analyzed using this optimal regularization methodology, and the results showed enhanced p values and area under the curve (AUC) for the task of differentiating malignant from benign lesions. Of the four absorption parameters and two scatter parameters, the most significant differences for benign versus malignant were total hemoglobin (HbT) and tissue optical index (TOI) with p values $= 0.01$ and 0.001, and AUC values $= 0.79$ and 0.94, respectively, in terms of HbT and TOI. This dramatically improved the values relative to fixed regularization (p value $= 0.02$ and 0.003; AUC $= 0.75$ and 0.83) showing that more differentiation was possible with the optimal method. Through a combination of both biomarkers, HbT and TOI, the AUC increased from 82.9% (fixed regulation $= 0.1$) to 94.3% (optimal method). [DOI: 10.1117/1.JBO.20.5.056009]

Keywords: diffuse optical tomography; near-infrared spectroscopy; regularization; image reconstruction.

Paper 140837RR received Dec. 15, 2014; accepted for publication Apr. 28, 2015; published online May 22, 2015.

1 Introduction

Magnetic resonance imaging (MRI)-guided near-infrared spectral tomography (NIRST) has been developed at just a few institutions, but has the potential to add molecular information to the spatial maps of MR imaging of the breast, and thereby increases the specificity of contrast-enhanced MRI exams.[1,2] In this imaging modality, the NIRST data measured at nine distinct wavelengths (ranging from 660 to 950 nm) and clinical MRI images are simultaneously acquired. Through model-based image recovery, the intrinsic biophysical composition of tissue can be estimated in terms of the concentrations of total hemoglobin (Hbt) and oxyhemoglobin, and the percentages of water and lipids.[3–5] Additionally, the ultrastructural cellular density and size ensemble associated with the extracellular matrix and subcellular constituents of breast tissue can be interrogated from the NIRST scattering spectrum. These parameters are spatially recovered according to anatomical regions identified from segmentation of the clinical breast MRI exams into regions of adipose, fibroglandular, and suspicious tissues.[6,7]

NIRST image recovery[8] is nonlinear and ill-posed and has been the subject of many years of research.[9–11] Reconstruction of the MRI/NIRST images requires the inversion of the Jacobian matrix, which encodes the spatial sensitivity to relative changes in the absorbing and scattering parameters of all locations for each source and detector pair. A widely used approach to solve the inverse problem is the Newton-Raphson technique regularized by a modified Levenberg–Marquardt (LM) algorithm.[12,13] Using segmented regions from MRI dramatically reduces the ill-conditioning of the problem to the point where it is overdetermined if the optical properties of only three regions are recovered (adipose, fibroglandular, and lesion). Nonetheless, the diffuse propagation of NIRS light in tissue still generates a poorly conditioned matrix that requires inversion. By regularizing the matrix to be inverted, amplification of the effects of measurement noise on the inversion is reduced, although the resulting solution is modified. Thus, the choice of regularization value is of great importance and has been studied by many researchers.[10,14] High regularization values smooth the spatial modes contained in the resulting images and may yield inadequate contrast recovery of the real NIRS parameters, whereas low regularization values do not sufficiently inhibit the noise effects from being amplified in the inversion process. Implementation of a method to automate the choice of regularization is critical for patient imaging.[15–18] While methods to choose this parameter are automatically well established in computational studies, little investigation of how the selection influences the diagnostic performance of the imaging method in actual practice has been reported. In this study, optimization of the regularization parameter based on L-curve analysis was pursued in clinical MRI/NIRST imaging with the specific goal of retrospectively

*Address all correspondence to: Yan Zhao, E-mail: yan.zhao-2.th@dartmouth.edu

1083-3668/2015/$25.00

maximizing the discrimination between known malignant and benign breast scans.[14]

A classically defined L-curve optimization algorithm was developed for regularization parameter selection during image reconstruction of data from 25 patients collected in a clinical study of women with breast abnormalities (BI-RADS category 4-5) of unknown diagnosis at the time of the imaging exam. The methodology was also used to study NIRST reconstruction with either amplitude data or both amplitude and phase data acquired with a multichannel 100 MHz frequency-domain NIR spectroscopy system. The performance of the optimal regularization was compared to fixed regularization in this setting of differentiating malignant from benign breast abnormalities. To the best of our knowledge, this study represents the first time the effects of regularization have been investigated in MRI-guided NIRST based on a relatively large dataset of clinical exams with the goal of optimizing task-based discrimination.

2 Methods

2.1 *Human Subject Imaging*

The imaging protocol for human subject examination was approved by the Committee for the Protection of Human Subjects at Dartmouth College and at Xijing Hospital in Xi'an, China. Breast exams from a total of 25 patients with ACR 4 and 5 breast abnormalities were evaluated. Within these 25 patients, the breast abnormalities were pathologically confirmed as 16 being cancer and 9 as being benign conditions, respectively.

2.2 *Imaging System and Instrumentation*

The details of the NIRST system have been reported in a previous publication.[7] Light sources consisting of six intensity-modulated (100 MHz) and three continuous-wavelength (CW) laser diodes cover the wavelength range of 660–950 nm for estimating the four main chromophores of oxyhemoglobin, deoxyhemoglobin, water, and lipid in the breast. A set of 15 photomultiplier tube (PMT) detectors (H9305-3, Hamamatsu) recorded FD measurements at wavelengths shorter than 850 nm, and 15 silicon photodiode (PD) detectors (C10439-03, Hamamatsu) acquired CW data in the longer wavelength range (900–950 nm). The output of the PD module was directly coupled into a 16-bit 64-channel multifunction data acquisition (DAQ) board (NI-PCI 6031E, NI), while the output of each PMT was heterodyned to low frequency, and then amplified to be sampled by the same DAQ board at 4 kHz for FD measurements and 1 kHz for CW measurements. A mechanical switch multiplexed the laser sources and detectors to 16 different positions, yielding a total of 240 (16×15) measurements at each wavelength. A set of 16 MRI-compatible optical fiber bundles delivered source light to the tissue and collected the resulting signal transmissions. The complete system was controlled and automated through custom LABVIEW software. One complete set of measurements using all nine wavelengths was acquired in 12 min. The fibers were held on the breast through a specially designed triangular interface which matched well to most breast sizes for single plane imaging. For coregistering the optical imaging plane to MR images, fiducial markers were placed at the end of each fiber bundle. The plane of optical imaging was selected by the radiologist and nurse attendant according to the suspicious region in the breast which was diagnosed by conventional imaging prior to the NIRST/MRI exam session, and later confirmed by postoperative pathology. MRI scans and optical measurements were simultaneously performed. No interference between the two imaging modalities was evident.

2.3 *Magnetic Resonance Imaging–Guided Near-Infrared Spectral Tomography Parameter Recovery*

2.3.1 *Light propagation model*

Breast MR images were processed and data reconstructed using NIRFAST software,[19,20] an open source platform developed at Dartmouth. Here, the propagation of photons was approximated by the diffusion equation based on the diffusive nature of photons in biological tissues when elastic scattering dominates absorption, and the source–detector separation is greater than several scattering mean free paths. Calculation of the diffusion model frequency-domain data then follows from

$$-\nabla \cdot D(\mathbf{r})\nabla\Phi(\mathbf{r},\omega) + (\mu_a(\mathbf{r}) + i\omega/c)\Phi(\mathbf{r},\omega) = Q_o(\mathbf{r},\omega), \tag{1}$$

where an isotropic source, Q_0, with source frequency ω at position $\mathbf{r}$ delivers light through turbid media. Here, Φ represents the fluence rate at position $\mathbf{r}$ observed at frequency ω. Also, $\mu_a(\mathbf{r})$ is the optical absorption coefficient and $D(\mathbf{r})$ is the optical diffusion coefficient, which is defined as

$$D(\mathbf{r}) = \frac{1}{3[\mu_a(\mathbf{r}) + \mu_s'(\mathbf{r})]}, \tag{2}$$

where $\mu_s'(r)$ is the reduced scattering coefficient. From Eq. (1), the fluence rate is calculated based on the optical properties iteratively estimated via model inversion during which the difference between measured data and the model solution of light propagation through the medium is minimized by adjusting the desired optical properties. The initial estimates of NIRST properties are obtained by assuming the tissue is homogeneous and fitting the data to the model, a process which has historically provided a reasonable starting point for the image reconstruction algorithm.

2.3.2 *Model inversion*

The optical properties are recovered during the model inversion through a modified-Tikhonov minimization, which is often used to stabilize ill-conditioned linear systems of equations. The objective equation used to minimize can be written as

$$\chi^2 = \left\{ \sum_{i=1}^{\mathrm{NM}} (\Phi_i^M - \Phi_i^C)^2 + \lambda \sum_{j=1}^{\mathrm{NN}} (\mu_j - \mu_0)^2 \right\}, \tag{3}$$

where Φ_i^M and Φ_i^C represent the measured and calculated data, respectively. NM is the number of measurements, and NN represents the number of optical parameter estimates. μ_0 symbolizes the initial estimates of NIRS properties in the tissue obtained from the homogeneous fit. Here, λ is the regularization parameter which balances the relative magnitudes of the two parts of the objective function— the data-model mismatch is represented by the first term, and the difference between the current estimates of optical properties and the initial starting values is expressed by the second term. A Newton-type LM procedure is utilized to produce the iterative update equation

$$(J^T J + \bar{\lambda} I)^{-1} J^T \delta\Phi = \delta\mu, \tag{4}$$

where J is the Jacobian matrix and I is the identity matrix. The update vector, $\delta\mu = \mu_i - \mu_0$, is obtained from the data-model mismatch, $\delta\phi$, in each iteration. Note that the ill-conditioned Hessian matrix, $J^T J$, is stabilized by adding the regularization term $2 * \lambda I$. Also, the Jacobian matrix can be constructed using amplitude data or both amplitude and phase data. The implications of this difference are further investigated in this paper, the choice of which depends on the detectors available for spectroscopic imaging. While amplitude and phase data would appear to provide a more complete sampling of the tissue, significant hardware benefits occur when using only amplitude data for spectroscopy, as will be discussed.

2.3.3 *Implementation of spatial priors*

Reduction of the recovered parameter space, μ, into a smaller number of larger regions segmented from MRI scans is known as encoding hard-prior information into the inversion.[11] In this study, the NIRST solutions were obtained with a three-dimensional image reconstruction algorithm[21] and prior information extracted from the coregistered breast MR images. Here, the assumption was made that the segmented regions from MRI—adipose, fibroglandular, and suspected tumor—had relatively homogeneous NIRS properties, and the goal of MRI/NIRST was to recover the corresponding region-based values. Additionally, spectral constraints were applied in the inversion through prior knowledge of the shapes of the absorbers' spectra and a presumed model for the elastic scattering spectra[22,23] to directly recover values for hemoglobin, deoxyhemoglobin, water, lipids, and scattering properties in each segmented breast region.

2.4 *Optimization of Regularization using L-Curve*

A common approach to selecting the regularization parameter, λ, is to use a fixed empirical number based on prior tissue-phantom studies, and to apply this value to data acquired from patient exams. In this study, an L-curve approach was used to find the optimal regularization parameter.[15,16] The L-curve is a parametric plot of the L-2 norm of the data-model mismatch $\rho(\lambda)$ versus the difference between optical properties of two iterations $\eta(\lambda)$, where

$$\rho(\lambda) = J\delta\mu - \delta\Phi, \tag{5}$$

$$\eta(\lambda) = \sum_{i=1}^{NN} (\mu_j - \mu_0)^2. \tag{6}$$

In other words, $\rho(\lambda)$ and $\eta(\lambda)$ represent the model-data error and spatial prior error, respectively, each of which is being minimized during the model inversion. With a relatively small λ, $\rho(\lambda)$ dominates the objective function, and a lower model error is expected at the cost of a larger prior error, and vice-versa for the case of large λ. Plotting $\rho(\lambda)$ versus $\eta(\lambda)$ for a range of λ illustrates the trade-off between these two types of errors, which typically exhibit an L-shaped curve. The corner of the L-curve is commonly regarded as the optimal regularization[16] because it minimizes the two error terms. In this study, the L-curve method was applied to determine the optimal regularization at each iteration.

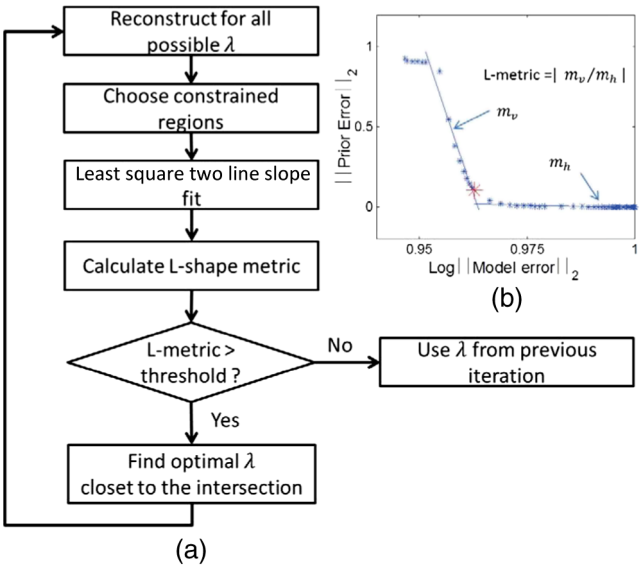

Fig. 1 (a) Flowchart outlining the sequence for the optimization algorithm. (b) The L2 norm of the prior property error versus L2 norm of the model error creates the L-curve of values for each regularization parameter values from 0.001 to 100. The optimization algorithm is implemented at each iteration, and optimal regularization parameter from previous iteration is used once the L metric falls behind the threshold.

Figure 1(a) outlines the sequence for optimization of regularization based on L-curve analysis at each iteration. To begin, prior error, which is the difference in optical property solutions between two iterations, is plotted versus model error over a range of discrete regularization values from 0.001 to 100. Figure 1(b) shows a typical L-curve at the first iteration of image reconstruction for a patient with a malignant breast abnormality. Here, the prior error, $\eta(\lambda)$, is defined as the difference of the sum of squared reconstructed optical parameters between the first iteration and initial estimate. The model-data mismatch, $\rho(\lambda)$, depicts the model error in the first iteration. When regularization increases, the model error increases and prior error decreases. Next, constrained regions are selected. In the range of regularization values from 0.001 to 0.02, the behavior of the prior error versus model error does not show a linear relationship because a small regularization results in unstable solutions in the ill-conditioned inverse problem. Once the constrained regions are selected, the L-curve can be fitted through least squares to slopes of m_v and m_h for vertical and horizontal regions, respectively, and a point on the L-curve with a maximal second derivative can be obtained. If this L-metric is larger than a threshold, an optimal regularization is assigned as the point which is closest to the intersection of the two fitting lines. Otherwise, the fitting at this iteration is discarded, and the optimal regularization value from the previous iteration is retained. The algorithm is repeated for each iteration until the stopping criterion for image reconstruction is satisfied.

2.5 *Image Reconstruction*

The combined CW/FD data acquisition provides amplitude and phase recordings from FD measurements involving six wavelengths, and amplitude data from CW measurements involving three wavelengths. Using the amplitude and phase data from the six wavelengths, the absorption and scattering coefficients at

each wavelength were estimated from homogeneous fitting to obtain the initial estimates of oxyhemoglobin (HbO), deoxyhemoglobin (Hb), water, lipid, scattering amplitude (SA), and scattering power (SP). Using the anatomical information provided by the MR images, computational meshes were created for the whole breast consisting of three regions composed of adipose, fibroglandular, and suspected tumor tissue. Each region was assumed to have uniform optical properties, and the absorption and scattering parameters were estimated for all three regions. From the recovered chromophores' concentrations, physiologically relevant parameters were calculated, including total hemoglobin HbT = HbO + Hb, oxygen saturation StO_2 = HbO/HbT, and tissue optical index TOI = HbT × Water/Lipid. Optical property contrast, defined as the ratio of the suspected tumor to background (adipose) properties, was used to differentiate malignant from benign abnormalities. Amplitude data (Ampl) and both amplitude and phase data (Ampl/Ph) were used for optical image reconstruction, respectively, to assess the relative performance of the two forms of data for the diagnostic task evaluated here (discriminating malignant from benign regions of interest).

2.6 *Statistical Analysis*

A Student's *t* test was used to determine whether malignant from benign lesions could be differentiated given the clinical exam data. Significance was achieved at the 95% confidence interval using a two-tailed distribution. To evaluate differences in differentiation of malignant versus benign lesions, receiver-operating characteristic (ROC) curve analysis was carried out by sweeping the threshold across the parameter space and estimating the sensitivity and specificity for detection of malignant versus benign breast scans. Area under the curve (AUC) is traditionally desired to be as close to unity as possible for the optimum test statistic.[24,25]

3 Results

Posthoc analysis performed using Tukey's HSD test revealed significant differences between optical property contrast when using a fixed regularization of 1 compared to using a fixed regularization of 0.1 ($p < 0.001$), and using a fixed regularization of 1 compared to optimal regularization ($p < 0.05$).

Figure 2 shows the recovered images of HbT, StO_2, water, lipid, SA, and SP of a patient with a biopsy-confirmed breast malignancy. The tumor-to-adipose contrasts of HbT, StO_2, water, lipid, SA, and SP were found to be 1.2, 1.1, 1.3, 1.6, 1.4, and 1.02, respectively. A fixed regularization parameter of 0.1 was used through the image reconstruction procedure for this patient.

Figure 3 shows the tumor-to-adipose contrast in HbT versus regularization for benign and malignant patients when images were estimated from amplitude data only, and box plots of HbT contrast in the two diagnostic groups for fixed regularization parameters of either 0.1 or 1, respectively. Compared to the malignant group, the HbT contrast was less sensitive to variation in regularization in the benign group, especially over the range of values from 0.01 to 0.2. Larger separation or difference in mean HbT contrast, between the malignant and benign groups resulted from the lower regularization of 0.1, even though less variation occurred within the same groups with a higher regularization of 1, although a statistically significant difference existed between the means of the malignant and benign groups with p values < 0.05 in either case.

Figure 4 shows the L-curves for the first three iterations during optical image reconstruction of a patient with a malignant

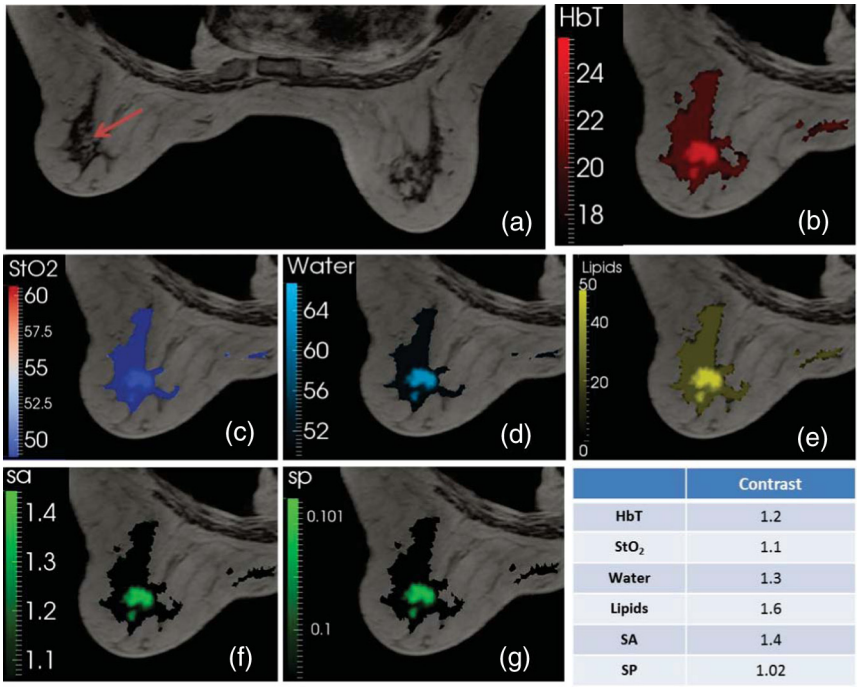

	Contrast
HbT	1.2
StO_2	1.1
Water	1.3
Lipids	1.6
SA	1.4
SP	1.02

Fig. 2 Images from a 33-year-old patient with a 11 × 21 × 14-mm^3 biopsy-confirmed invasive ductal carcinoma (IDC) in her right breast. (a) Noncontrast T1 MRI with tumor location indicated (arrow); (b) Reconstructed images for total hemoglobin (HbT), (c) oxygen saturation (StO_2), (d) water, (e) lipid, (f) scattering amplitude (SA), and (g) scattering power (SP) is overlaid on the MR scan. The value of each parameter in the adipose region is suppressed for clarity of visualization.

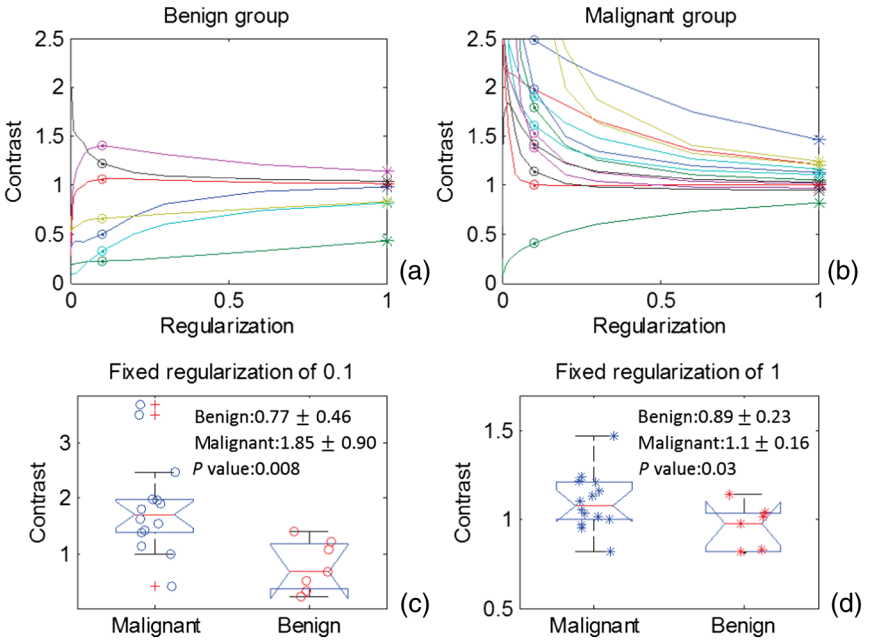

Fig. 3 Tumor-to-adipose contrast in HbT versus regularization for (a) benign, and (b) malignant cases. Circles have a regularization of 0.1, and asterisks have a regularization of 1. Box plots of contrast for the two pathologies are shown with fixed regularizations of (c) 0.1 and (d) 1 for all patients.

breast abnormality. The same range of regularization values (0.001 to 100) was used to plot the L-curve at each iteration. Both the range of model error and prior error decrease with an increasing number of iterations. Optimization of regularization was implemented using the algorithm outlined in Fig. 1(a); the optimal point is marked by a red asterisk in the first two iterations and had values of 0.18 and 0.22, respectively. At the third iteration, the L-curve metric was below the threshold, and an optimal regularization could not be found using the same process. Instead, the regularization value for the third iteration was set to be the same as used in the second iteration, namely 0.22. The L-curves of the optical data acquired from most patient exams exhibited similar behaviors. The number of patient datasets which had an optimal regularization based on L-curve analysis was 22, 12, and 0 for the first three iterations. The average optimal regularization for the first and second iterations was 0.21 and 0.24, respectively. After three iterations, none of the exam data had an L-curve with a metric higher than the threshold.

The number of iterations used in the reconstruction was also an important factor. In Fig. 5(a), the projection error, which represents the residual of the inversion equation, is plotted on a log scale as a function of the number of iterations and decreases with an increasing number of iterations. The largest decrease in the projection error occurred at the first iteration, which is typical behavior for a Newton-type iterative method. The change in the projection error by the ninth iteration was relatively small, resulting in convergence of the tumor-to-adipose contrast as shown in Fig. 5(b). In this study, nine iterations were chosen as the stopping criteria for image reconstruction of all patients.

Table 1 summarizes the statistical and diagnostic results in terms of HbT and TOI contrast using fixed regularization values of 0.1 and 1, and optimal regularization based on L-curve analysis. Data from 22 patient exams which had an optimal regularization in the first iteration were included in the analysis. A significant difference ($p < 0.05$) was found in HbT contrast for malignant versus benign patients for all three regularization selections.

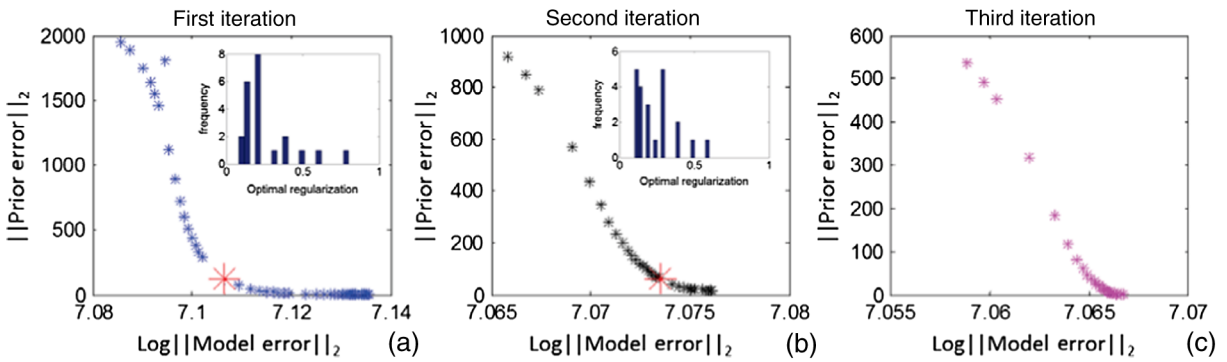

Fig. 4 L-curves are shown for the first three iterations of a single case with a malignant tumor. The regularization was varied from 0.001 to 100 at each iteration, and the optimal regularization was (a) 0.18, (b) 0.22, and (c) undefined for the three iterations, respectively.

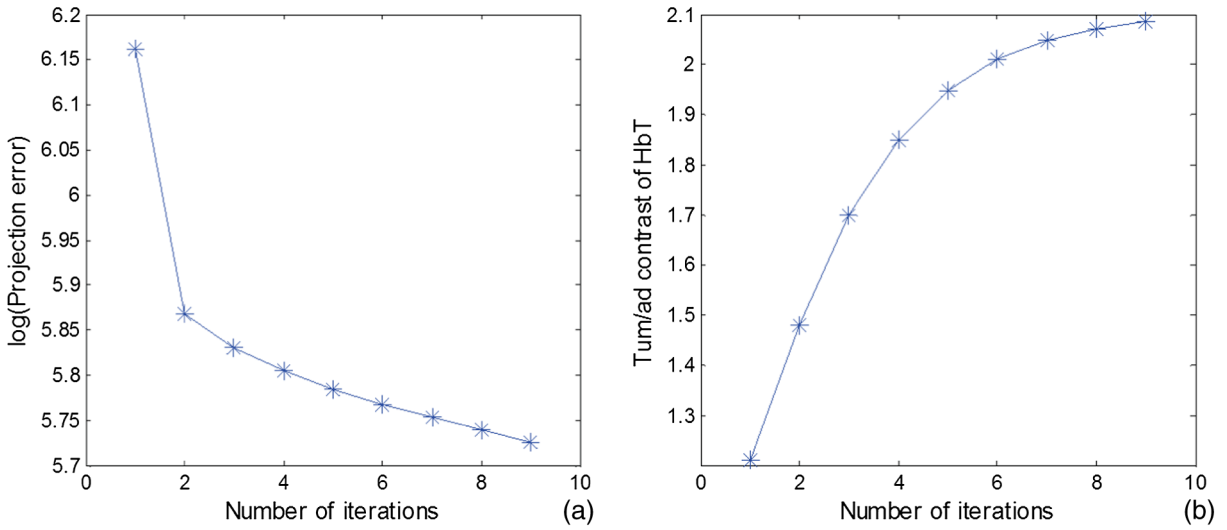

Fig. 5 (a) Log scale of projection error versus number of iterations. (b) Tumor-to-adipose contrast in HbT versus number of iterations.

Both amplitude and phase data were used in the image reconstruction to see if the involvement of phase data obtained at the six FD domain wavelengths further improved the accuracy of the optical image reconstruction.

Figure 6 is organized the same as Fig. 3, except that the reconstructions utilized both amplitude and phase data, and the three clinical exams that did not have an apparent optimal regularization value in the first iteration were excluded. In Figs. 6(a) and 6(b), the tumor-to-adipose contrast in HbT was plotted as a function of regularization for benign and malignant patients, respectively. When regularization decreased, the contrast increased in most cases. As a result, better separation occurred between the malignant and benign groups, although with a higher standard deviation at the lower regularization of 0.1 as shown in Figs. 6(c) and 6(d). Here, the HbT contrast in the benign group was more sensitive to the change in regularization for low values when compared with the results in Fig. 2(a). Apparently, determining an appropriate regularization for image reconstruction using both amplitude and phase data is even more important than when using only amplitude measurements.

We also applied the optimization algorithm (Fig. 1) during image reconstruction with both amplitude and phase data; but, L-curve analysis failed to find an optimal regularization. The compromise between model error and prior error was not significant on the L-curve at any point; hence, no optimal regularization parameter could be found that satisfied the criterion of the optimization algorithm. One approach to improve the L-metric might be to use separate regularization parameters for amplitude and phase data. In practice, we found that a fixed regularization of 2 for phase data, and an optimal regularization based on L-curve analysis for amplitude data worked well.

Table 2 summarizes the statistical results of 22 patient exams, in which the optimal regularization (on amplitude only, phase fixed at 2) was compared with fixed regularization values of 0.1 and 1, when both amplitude and phase data were used in the image reconstruction. Reconstruction using a fixed regularization of 0.1 for amplitude and 2 for phase data was compared as well. Significant differences ($p < 0.05$) exist between the malignant and benign groups in terms of both HbT and TOI for either a fixed regularization of 1 or optimal regularization. Optimal regularization provides the highest AUC for TOI (0.94) among all the regularization choices. Meanwhile, the optimization method still gives a relatively high AUC for HbT, without a significant difference compared with the fourth approach. To summarize, the optimization technique provides a systematic and automated way to find the optimal regularization parameter in each iteration, which gives the best separation between malignant and benign groups in terms of recovered optical parameter TOI. The L-curve-based optimization technique utilized in this paper aims at finding the tradeoff between prior error and model error in terms of Hb and deoxy-Hb, water, and lipids. As a result, the increase of AUC for TOI is more obvious than HbT

Table 1 Comparison of statistics using fixed regularization of 0.1 and 1, and optimal regularization. Only amplitude data (AMPL) was used for image reconstruction.

	Total hemoglobin				Tissue optical index			
	Malignant	Benign	*P*-value	AUC	Malignant	Benign	*P*-value	AUC
AMPL $\lambda = 0.1$	1.78 ± 0.89	0.77 ± 0.46	0.01[a]	0.83	1.34 ± 1.23	0.31 ± 0.17	0.005[a]	0.91
AMPL $\lambda = 1$	1.08 ± 0.17	0.89 ± 0.23	0.04[a]	0.71	1.11 ± 0.23	0.79 ± 0.20	0.006[a]	0.90
AMPL optimal λ	1.46 ± 0.51	0.86 ± 0.36	0.01[a]	0.81	1.26 ± 1.08	0.43 ± 0.17	0.06	0.93

[a]Significant difference as defined by p value < 0.05

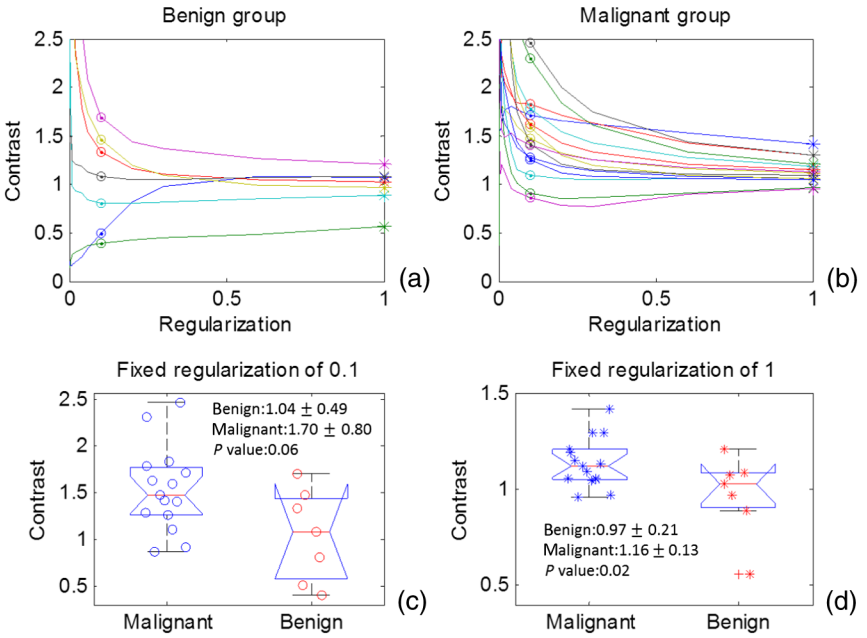

Fig. 6 Tumor-to-adipose contrast of HbT versus regularization for (a) benign conditions and (b) malignant tumors. Circles have a regularization of 0.1, and asterisks have a regularization of 1. Box plots of contrast are shown for regularizations of (c) 0.1, and (d) 1 for all patients. Both amplitude and phase data were used in the image reconstructions.

Table 2 Comparison of statistics using fixed regularization of 0.1 and 1, optimal regularization, and fixed regularization of 0.1 for amplitude and 2 for phase. Both amplitude and phase data (AMPL/PH) were used for image reconstruction.

	Total hemoglobin				Tissue optical index			
	Malignant	Benign	*P*-value	AUC	Malignant	Benign	*P*-value	AUC
AMPL/PH $\lambda = 0.1$	1.70 ± 0.80	1.04 ± 0.49	0.06	0.74	1.30 ± 1.14	0.54 ± 0.39	0.10	0.73
AMPL/PH $\lambda = 1$	1.16 ± 0.13	0.97 ± 0.21	0.02[a]	0.75	1.17 ± 0.21	0.88 ± 0.19	0.003[a]	0.83
AMPL/PH optimal λ	1.54 ± 0.52	0.95 ± 0.36	0.01[a]	0.79	1.13 ± 0.44	0.49 ± 0.18	0.001[a]	0.94
AMPL $\lambda = 0.1$/PH $\lambda = 2$	1.88 ± 0.90	0.90 ± 0.45	0.01[a]	0.83	1.53 ± 1.49	0.38 ± 0.18	0.06	0.88

[a]Significant difference as defined by p value < 0.05

compared with fixed regularization, since TOI (HbT × Water/Lipid) is defined such that it represents all the recovered chromophore concentrations. Interestingly, the addition of phase information appears to degrade the statistical performance of the image reconstructions in the fixed regularization cases.

Instead of using a single predictor, either HbT or TOI, we evaluated the combination of HbT and TOI as an indicator of malignant versus benign contrast-enhancing MRI regions of interest. Specifically, we applied both HbT and TOI as predictors, and fit a logistic regression using pathology-confirmed malignancy to obtain the outcome. The predicted score from the logistic regression model was used to construct the ROC curve.[26] We repeated this procedure for three different regularization parameters and compared their AUCs with a bootstrapping method.[27] As shown in Fig. 7, under these conditions, the optimal regularization improved the AUC (94.4%), relative to the fixed regularizations of 0.1 (88.2%) or 1 (84.4%).

Figure 8 presents the boxplots of tumor-to-adipose contrast for (a) HbT, (b) StO_2, (c) TOI, (d) SA, and (e) SP by applying the optimization algorithm during image reconstruction with amplitude and phase data. HbT was the most significant indicator for differentiating the malignant and benign groups, and provided the largest mean difference in tumor-to-adipose contrast in the malignant and benign groups (1.55× versus 0.89×). A significant difference in TOI and SP contrast was also observed. The average contrast in both HbT and TOI was significantly higher in the malignant group than in the benign group. No significant difference in the StO_2 contrast was found.

4 Discussion

The results presented in this paper show that the contrasts recovered in both HbT and TOI were diagnostically significant, but also depended on the choice of regularization parameter. Thus, an objective methodology to select/identify the regularization parameter for reconstructing data from individual patient exams is critical for practical application of the combined MRI/NIRST imaging approach in the clinical diagnostic setting. Instead of applying an empirical value for every subject exam,

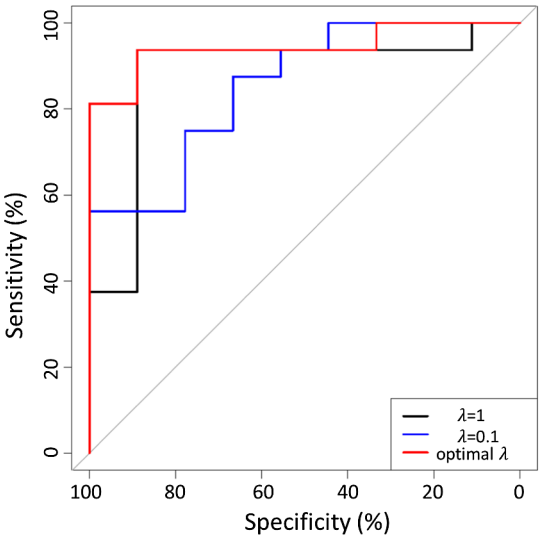

Fig. 7 Receiver-operating characteristic (ROC) curve for fixed regularization of 1 (black) and 0.1 (blue), and optimal regularization (red), when HbT and TOI are combined. Both amplitude and phase data were used for image reconstruction.

the optimization algorithm sought an exam-specific regularization parameter (or series of parameters) for image reconstruction that was derived from the measured optical data. The optimization algorithm developed and applied here was based on L-curve analysis, which is widely used to stabilize ill-conditioned problems by balancing the model error with the prior error as constrained by the prior information. However, previous approaches of finding the "elbow" on the L-curve have been primarily limited to theoretical or simulation studies with few efforts being based on actual patient data. To deal with an L-curve generated from clinical exam data, we defined a metric describing the characteristics of the resulting L-shape, and developed an optimization approach based on least-square fitting of the response. The L-metric determined whether the L-curve was sufficient for selecting an optimal regularization parameter, and if so, the optimal value from the curve was utilized. Otherwise, the value from the previous iteration remained. The optimization algorithm appeared to be robust and effective in the clinical dataset we applied. We found that the average L-metric of all exams decreased with increasing number of iterations (although the number of iterations was set to 9 in all cases, i.e., we did not apply the L-metric or L-curve as a stopping criterion). Within four iterations, the projection error and measurement noise amplification were balanced and the contrast converged. Table 1 showed the comparisons of the diagnostic statistics resulting from three choices of regularization parameters. Moreover, although StO_2 or scattering properties were not found to be significant indicators when taken alone, their values when used to form TOI contributed to the optimal indicator for differentiation of malignant from benign lesions.

When the regularization parameter decreased, less dependence in the recovered optical solution occurred with the prior information. The prior estimate was obtained under the assumption that the whole breast had the same optical properties. As a result, higher regularization will lower the contrast between tumor and background leading to a smaller separation in the mean HbT and TOI contrast between the malignant and benign diagnostic groups at a regularization of 1. On the other hand, a high regularization also suppresses the high spatial frequency variation in the recovered optical property distribution resulting from measurement noise, and produced lower variation in HbT and TOI within the malignant and benign groupings. A compromise between separation of the mean value and noise driven variability was obtained by applying the optimal regularization approach during image reconstruction.

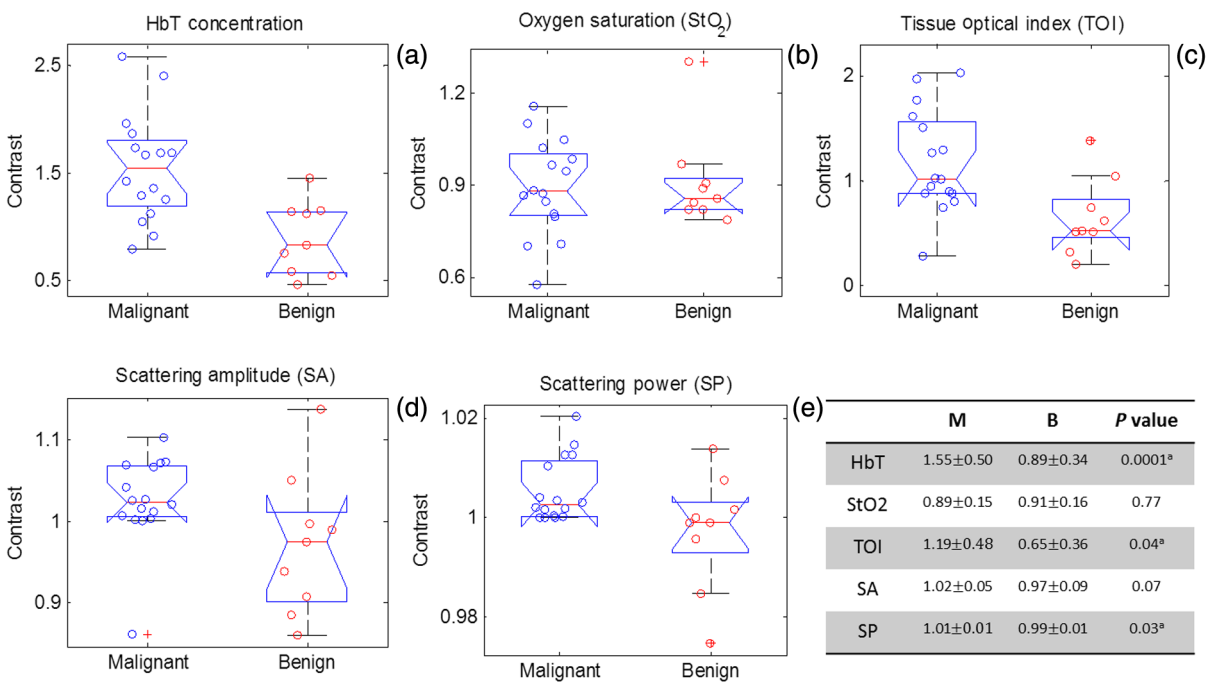

	M	B	*P* value
HbT	1.55±0.50	0.89±0.34	0.0001[a]
StO2	0.89±0.15	0.91±0.16	0.77
TOI	1.19±0.48	0.65±0.36	0.04[a]
SA	1.02±0.05	0.97±0.09	0.07
SP	1.01±0.01	0.99±0.01	0.03[a]

Fig. 8 Box plots of the contrast for: (a) HbT, (b) StO_2, (c) tissue optical index (TOI), (d) scattering power (SA), and (e) scattering power (SP), as recovered using the optimal regularization and amplitude and phase data. [a]Significant difference.

Table 3 Comparison of the three regularization approaches in all clinical exams, relative to selected exams when the optimal regularization parameter was found. The group of all exams included 16 malignant and 9 benign pathology-confirmed diagnoses, whereas the selected exams included 15 malignant and 7 benign cases (three exams from the former did not have optimal regularization at the first iteration). Both amplitude and phase data were used during image reconstruction.

	Total hemoglobin				Tissue optical index			
	All patients		Selected patients		All patients		Selected patients	
	P-value	AUC	*P*-value	AUC	*P*-value	AUC	*P*-value	AUC
AMPL/PH $\lambda = 0.1$	0.02[a]	0.79	0.06	0.74	0.16	0.63	0.10	0.73
AMPL/PH $\lambda = 1$	0.004[a]	0.79	0.02[a]	0.75	0.001[a]	0.84	0.003[a]	0.83
AMPL/PH optimal λ	0.002[a]	0.81	0.01[a]	0.79	0.009[a]	0.78	0.001[a]	0.94

[a]Significant difference as defined by p value < 0.05.

We also investigated the effects of optimal regularization on the recovered optical image when both amplitude and phase data were used (relative to only amplitude measurements). In this case, the regularization algorithm failed to find an optimal value based on L-curve analysis, apparently because the relative contribution of phase data noise was higher than amplitude data noise, requiring much higher regularization of the phase data. Here, separate regularization values for phase and amplitude data improved the resulting image outcomes. Specifically, improvement occurred when regularization of the amplitude data was obtained through L-curve analysis, and regularization of the phase data was fixed at 2 (~1 order of magnitude higher than the value used in the amplitude regularization). With this approach, improvement in diagnostic performance in terms of higher AUC for both HbT and TOI occurred relative to using fixed regularization. When the phase data were added to the Jacobian matrix for image reconstruction, the optimal regularization (with separate but fixed phase regularization) achieved maximal separation of the malignant from benign diagnoses (highest AUC). Finally, the optimal regularization generated the best AUC value (0.94) relative to the other regularization choices considered when HbT and TOI were combined as the diagnostic indicator (Fig. 7).

Although the best diagnostic performance occurred using both amplitude and phase data, the three regularization approaches, either fixed or optimal, were still able to separate the malignant and benign groups in terms of HbT ($p < 0.05$), when applying only amplitude data for image reconstruction. These results suggest the possibility of simplifying the MRI/NIRS system into one with only CW channels, which would significantly reduce costs while not sacrificing much in terms of diagnostic performance.

In the results presented here, data acquired in 22 out of 25 patient exams had an optimal regularization parameter identified by L-curve analysis in the first iteration and were included in the statistical analyses. For completeness, we compared the outcomes of the optimization algorithm in all 25 patients in Table 3 in terms of the p value and AUC for HbT and TOI contrast when applying the three regularization approaches. Both amplitude and phase data were used for image reconstruction in these results. For the subset of selected patients (22), optimal regularization provided the best AUC for both TOI and HbT relative to fixed regularization, but only for HbT when all exam data were evaluated. Thus, the L-curve approach may be a pragmatic way to identify which clinically acquired datasets are reliable. NIRS data can be compromised by a number of factors during their acquisition, such as fiber-tissue coupling or reflections; hence, the ability to objectively and conclusively determine which datasets will not lead to accurate spectroscopic parameter recovery could be important in clinical practice.

5 Conclusion

In this work, a robust optimization algorithm for selection of the regularization to be applied during image reconstruction based on exam-specific data acquired during MRI/NIRST examination of the breast was developed. The optical contrast values for HbT, StO_2, TOI, and scattering parameters were estimated by applying the optimization algorithm when amplitude only and both amplitude and phase data. A statistical difference ($p < 0.05$) occurred between malignant and benign groups for both absorption-derived contrasts (HbT and TOI) as well as reduced-scattering derived contrast (SP).

To the best of our knowledge, these results represent the first time an extensive study of regularization has been conducted on a relatively large amount of clinical breast exam data with the MRI/NIRST multimodality imaging approach. The optimization algorithm better differentiated malignant from benign cases compared to a fixed regularization parameter. The best diagnostic performance occurred with optimal regularization values selected from the individual's exam data, and when combining HbT and TOI estimated from both amplitude and phase data as the diagnostic indicator.

Acknowledgments

This work was funded by NIH Grant No. R01 CA069544 and National Natural Science of China No. 81101091. We kindly thank Dr. Venkataramanan Krishnaswamy and Dr. Robert Holt for their advice.

References

1. V. Ntziachristos et al., "MRI-guided diffuse optical spectroscopy of malignant and benign breast lesions," *Neoplasia* **4**, 347–354 (2002).
2. B. J. Tromberg et al., "Assessing the future of diffuse optical imaging technologies for breast cancer management," *Med. Phys.* **35**, 2443–2451 (2008).
3. D. Hsiang et al., "In vivo absorption, scattering, and physiologic properties of 58 malignant breast tumors determined by broadband diffuse optical spectroscopy," *J. Biomed. Opt.* **11**, 044005 (2006).

4. A. Corlu et al., "Three-dimensional in vivo fluorescence diffuse optical tomography of breast cancer in humans," *Opt. Express* **15**, 6696–6716 (2007).
5. B. W. Pogue et al., "Characterization of hemoglobin, water, and NIR scattering in breast tissue: analysis of intersubject variability and menstrual cycle changes," *J. Biomed. Opt.* **9**, 541–552 (2004).
6. M. A. Mastanduno et al., "Adaptable near infrared spectroscopy fiber array for improved coupling to different breast sizes during clinical MRI," *Acad. Radiol.* **21**, 141–150 (2014).
7. F. El-Ghussein et al., "Hybrid photomultiplier tube and photodiode parallel detection array for wideband optical spectroscopy of the breast guided by magnetic resonance imaging," *J. Biomed. Opt.* **19**, 011010 (2014).
8. S. R. Arridge, "Optical tomography in medical imaging," *Inv. Problems* **15**, R41–R93 (1999).
9. J. R. Singer et al., "Image reconstruction of the interior of bodies that diffuse radiation," *Science* **248**, 990–993 (1990).
10. B. W. Pogue et al., "Spatially variant regularization improves diffuse optical tomography," *Appl. Opt.* **38**, 2950–2961 (1999).
11. P. K. Yalavarthy et al., "Weight-matrix structured regularization provides optimal generalized least-squares estimate in diffuse optical tomography," *Med. Phys.* **34**, 2085–2098 (2007).
12. S. R. Arridge et al., "Reconstruction methods for infrared absorption imaging," *Proc. SPIE* **1431**, 204–215 (1991).
13. K. D. Paulsen and H. Jiang, "Spatially varying optical property reconstruction using a finite element diffusion equation approximation," *Med. Phys.* **22**, 691–701 (1995).
14. A. Li et al., "Tomographic optical breast imaging guided by three-dimensional mammography," *Appl. Opt.* **42**, 5181–5190 (2003).
15. P. C. Hansen, "Truncated singular value decomposition solutions to discrete ill-posed problems with ill-determined numerical rank," *SIAM J. Sci. Stat. Comput.* **11**, 503–518 (1990).
16. P. C. Hansen, "Analysis of discrete ill-posed problems by means of the L-curve," *SIAM Rev.* **34**, 561–580 (1992).
17. J. P. Culver et al., "Three-dimensional diffuse optical tomography in the parallel plane transmission geometry: evaluation of a hybrid frequency domain/continuous wave clinical system for breast imaging," *Med. Phys.* **30**, 235–247 (2003).
18. R. J. Gaudette et al., "A comparison study of linear reconstruction techniques for diffuse optical tomographic imaging of absorption coefficient," *Phys. Med. Biol.* **45**, 1051–1070 (2000).
19. M. Jermyn et al., "Fast segmentation and high-quality three-dimensional volume mesh creation from medical images for diffuse optical tomography," *J. Biomed. Opt.* **18**, 086007 (2013).
20. H. Dehghani et al., "Near infrared optical tomography using NIRFAST: algorithm for numerical model and image reconstruction," *Commun. Numer. Methods Eng.* **25**, 711–732 (2009).
21. C. M. Carpenter et al., "Inspired gas induced vascular change in tumors with MR-guided near-infrared imaging: a human breast pilot study," *J. Biomed. Opt.* **15**, 036026 (2010).
22. S. Srinivasan et al., "Spectrally constrained chromophore and scattering near-infrared tomography provides quantitative and robust reconstruction," *Appl. Opt.* **44**, 1858–1869 (2005).
23. A. Corlu et al., "Diffuse optical tomography with spectral constraints and wavelength optimization," *Appl. Opt.* **44**, 2082–2093 (2005).
24. C. E. Metz, "Basic principles of ROC analysis," in *Proc. Seminars in nuclear medicine*, pp. 283–298, WB Saunders (1978).
25. J. A. Swets, "Measuring the accuracy of diagnostic systems," *Science* **240**, 1285–1293 (1988).
26. J. Carpenter and J. Bithell "Bootstrap confidence intervals: when, which, what? A practical guide for medical statisticians," *Stat. Med.* **19**, 1141–1164 (2000).
27. E. R. DeLong, D. M. DeLong, and D. L. Clarke-Pearson, "Comparing the areas under two or more correlated receiver operating characteristic curves: a nonparametric approach," *Biometrics* **44**, 837–845 (1988).

Yan Zhao received his BS degree in electronic science and technology from Xi'an Jiaotong University, Xi'an, China, in 2012. Currently, he is working toward his PhD from Thayer School of Engineering, Dartmouth College in Hanover, New Hampshire, United States. His research interests include biomedical spectroscopy and image reconstruction.

Biographies for the other authors are not available.